JOURNAL OF SOLID STATE CHEMISTRY **124,** 43–51 (1996)
ARTICLE NO. 0205

Effect of Nonstoichiometry on Properties of $La_{1-t}MnO_{3+\delta}$

III. Magnetic Order Studied by Powder Neutron Diffraction

Bjørn C. Hauback,* Helmer Fjellvåg,† and Natsuko Sakai†,[1]

*Institutt for energiteknikk, N-2007 Kjeller, Norway; and †Department of Chemistry, University of Oslo, N-0315 Oslo, Norway

Received October 23, 1995; in revised form February 26, 1996; accepted February 28, 1996

The magnetic order, moments, and ordering temperatures for $La_{1-t}MnO_{3+\delta}$ depend strongly on its nonstoichiometry. Powder neutron diffraction samples were obtained via precursor based synthesis, annealing in atmospheres with controlled oxygen partial pressures, and adequate quenching or slow cooling. The samples are representative for most of the nonstoichiometric domain. Three modifications of $La_{1-t}MnO_{3+\delta}$ were studied. First, the reduced phase with Jahn–Teller deformed Mn^{III} is orthorhombic (ORT1) and orders antiferromagnetically (A_x mode), typically $T_N \approx 140$ K and $\mu_{AF} \approx 3.4\ \mu_B$ ($0.00 \leq t \leq 0.08$). All samples of this type exhibit parasitic ferromagnetism. Second, the fully oxidized samples have average Mn oxidation state around 3.2, and have rhombohedral (RH) crystal structure with ferromagnetic order at low temperatures; $T_C \approx 213 \pm 10$ K and $\mu_F = 3.9 \pm 0.1\ \mu_B$ for $La_{0.96}MnO_{3.05}$. Third, for intermediate oxygen contents an orthorhombic structure (ORT2) occurs, with minor distortions of the MnO_6-octahedra. For $LaMnO_{3.08}$ of ORT2-type, ferromagnetic order (F_y mode) occurs below $T_C = 125 \pm 10$ K. The ordered magnetic moment, $\mu_F = 2.46 \pm 0.04\ \mu_B$ is rather small. $LaMnO_{3.15}$ also takes the ORT2-type structure at low temperature, as proved by weak superstructure reflections. At 200 ± 20 K, $LaMnO_{3.15}$ undergoes a first order transition to the RH-type. The ordered magnetic moment, if present, is very small and in any case far from expectations for Mn^{III}/Mn^{IV} mixtures. It is proposed that the approximately 3 : 1 ratio between Mn^{III} and Mn^{IV} atoms in $LaMnO_{3.15}$ gives rise to a frustrated system with largely spin glass behaviour.

INTRODUCTION

The first studies of magnetic order in lanthanum manganese (III) oxide, $LaMnO_3$ (lanthanum manganite), including its solid solution derivatives, were performed during the early days of the powder neutron diffraction technique (1, 2). However, during these studies little attention was paid to the possibility of detailed monitoring of the valence state of manganese by controlled variation of the nonstoichiometry. Many early studies were hampered by low resolution in the diffraction profiles, which caused ambiguity with regard to the crystallographic state. The present powder neutron diffraction (PND) study aims at extending the knowledge on the effect of nonstoichiometry and structural deformation on the magnetic order of perovskite type $La_{1-t}MnO_{3+\delta}$.

The magnetic order (G, A, C, and F type) in deformed perovskite type oxides of the transition elements has been subject to numerous studied (3–5). Stoichiometric $LaMnO_3$ exhibits layer-like antiferromagnetic order of A_x-type; *i.e.,* the ferromagnetically coupled spins within *ac*-planes (space group *Pnma*) are antiferromagnetically coupled along **b**. In the literature, the Néel temperature for $LaMnO_3$, T_N, varies between 100 and 141 K (1, 3, 6). The ordered magnetic moment is $3.9 \pm 0.2\ \mu_B$ (2). The observed coexistence of weak parasitic ferromagnetism has been ascribed as an intrinsic effect resulting from oxygen excess (7–11) and $LaMnO_3$ has acted as a model compound for discussion of the effect of mobile carriers in antiferromagnetic materials (10, 11).

The structural state and physical properties of perovskite related oxides are susceptible to changes in the oxygen nonstoichiometry, the range of which may be extended by adopting high pressure techniques, electrochemical methods or topotactic reductions (12–14). Lanthanum manganite is rather extraordinary in showing oxidative nonstoichiometry under normal conditions, which structurally implies cation vacancies (15–17). Although the formula $La_{1-t}MnO_{3+\delta}$ is adopted here and considered to cover all defect situations, reformulation into $La_{(3-3t)/(3+\delta)}Mn_{3/(3+\delta)}O_{3-x}$ is more appropriate on a crystallographic basis ($x > 0$ for large La deficits and/or reducing conditions). The nonstoichiometry in $La_{1-t}MnO_{3+\delta}$ and its effect on transport properties has repeatedly been studied as function of temperature and oxygen partial pressure (17–21).

In parts I and II of this study (21, 22) the existence range,

[1] Current address: Department of Inorganic Materials, National Institute of Materials and Chemical Research, 1-1 Higashi, Tsukuba, Ibaraki 305, Japan

0022-4596/96 $18.00

phase relations, and crystal structure for $La_{1-t}MnO_{3+\delta}$ were considered. The present neutron diffraction study aims at establishing correlations between magnetic order, crystal structure, and nonstoichiometry, and covers representative samples throughout the entire nonstoichiometric region. Rather extreme situations are included; $LaMnO_{3.15}$ with 5% vacancies in the Mn and La sites and with 30% of the total manganese converted from Mn^{III} to Mn^{IV}; $LaMnO_3$, the stoichiometric phase with 100% Mn^{III}; and $La_{0.92}Mn O_{2.98}$, with a filled Mn-sublattice with 20% Mn^{IV} and vacancies at the La and O sites. The PND samples represent three types of deformed perovskite type structures—one rhombohedral (RH-type) and two orthorhombic (ORT1- and ORT2-types). This study is not completely exhaustive since all interesting compositions could not be investigated by PND; a detailed mapping of the magnetic phase diagram for $La_{1-t}MnO_{3+\delta}$ is provided in Part IV (23). The present study is restricted to samples annealed at high temperatures under selected temperature (T)–oxygen partial pressure [$p(O_2)$] conditions, thereafter either being quenched or slowly cooled to room temperature in air or in reducing atmosphere.

EXPERIMENTAL

Large samples (10–20 g) of $La_{1-t}MnO_{3+\delta}$, $t = 0.00$, 0.04, 0.08, and 0.12, were prepared for the powder neutron diffraction study, starting with mixtures of titrated aqueous solutions of $LaCl_3$ and $MnCl_2$. Addition of ammonium carbonate forced precipitation of $La_2(CO_3)_3$ and $MnCO_3$. After drying and washing, the carbonate mixture was calcined at 1373 K to provide a single phase oxide. Phase pure samples were obtained for $0.00 < t \leq 0.08$. Slight amounts of Mn_3O_4 were observed for $t = 0.12$. No indications of Mn_3O_4 were found in magnetic susceptibility data for $t \leq 0.08$ (ferromagnetic Mn_3O_4 has $T_C = 42$ K and $\sigma = 42$ emu/g at 5 K).

The oxygen content (δ) was monitored in a final heat treatment using tube furnaces and regulating the atmosphere. Moderate to high oxygen partial pressures were obtained by mixing oxygen and argon. Low oxygen partial pressures, $p(O_2) < 10^2$ Pa, were obtained in $H_2/CO_2/Ar$ gas mixtures. The oxygen potential in the exhaust gas was monitored by an oxygen sensor based on yttrium-stabilized zirconia. The required conditions were determined separately from TGA studies. The oxygen contents of the samples were determined by means of complete reoxidation in pure oxygen using TGA (Perkin Elmer TGA7). The reoxidation is slow at room temperature and does not cause stability for the PND studies. For further details on the syntheses, see (14, 21).

Phase purity, homogeneity, and unit cell dimensions were determined from powder X-ray diffraction (PXD) at room temperature (Guinier–Hägg cameras, Cu$K\alpha_1$ or Cr$K\alpha_1$ radiation, Si internal standard (24)). Unit cell dimensions were obtained by least-squares calculations using the CELLKANT program (25).

Magnetic susceptibility data were recorded for zero field cooled (ZFC) samples with a SQUID magnetometer (MPMS, Quantum Design) between 5 and 300 K for applied magnetic fields (H) between 25 and 1000 Oe. Field cooled (FC) experiments were performed for $H = 1$ kOe. Magnetization data were recorded in fields up to 50 kOe and saturation magnetization was determined by $1/H$ extrapolation.

Powder neutron diffraction data were collected with the OPUS IV two-axis diffractometer at the JEEP II reactor, Kjeller. Cylindrical sample holders were used. Monochromatized neutrons of wavelength 182.5 pm were obtained by reflection from Ge(111). The scattered intensities were measured by five ^{3}He detectors, positioned 10° apart. Intensity data were collected from $2\Theta = 5$ to 100° in steps of $\Delta 2\Theta = 0.05°$. A typical data set contained 1700 measuring points, and some 25 (rhombohedral structure) to 80 (orthorhombic structure) reflections entered into the profile refinements. Temperatures between 9 and 300 K were obtained by means of a Displex cooling system. A Lake Shore DRC 82C controller was used, and the temperature was measured and controlled by means of a silicon diode.

Atomic coordinates, isotropic displacement factors, and magnetic moments were obtained from Rietveld-type refinements. The Hewat version of the Rietveld program (26, 27) was used. Regions with reflections from Al of the Displex were excluded. One scale factor, three half width parameters, three (two) unit cell dimensions and a zero point, seven (one) positional parameters, and three (two) occupation numbers, together with one overall isotropic displacement factor and three (two) components for the magnetic structure, entered into the least-squares refinements for the orthorhombic (rhombohedral) structures. The scattering amplitudes $b_{La} = 8.27$, $b_{Mn} = -3.73$, and $b_O = 5.805$ fm (28) were used together with form factors for Mn^{3+} (29). The magnetic scattering for the rhombohedral phases was calculated according to a uniaxial model.

RESULTS AND DISCUSSION

(*i*) *Structural and magnetic characterization of PND samples.* Synthesis conditions, oxygen contents and unit cell dimensions for the PND samples of $La_{1-t}MnO_{3+\delta}$ are listed in Table 1. Samples prepared under strongly reducing conditions (typically $p(O_2) = 10^{-7}$ Pa; CO_2/H_2 at 1270 K) contain solely/mainly Mn^{III} and take a Jahn–Teller distorted variant (ORT1) of the $GdFeO_3$-type structure. Samples equilibrated and slowly cooled in air from 1000 K contain substantial amounts of Mn^{IV} and take the rhombohedral $LaAlO_3$-type structure (RH). The third category, the ORT2-type samples, are found for samples quenched

TABLE 1

Stoichiometry (*Nominal* La/Mn Ratio, $1 - t$, and Analyzed Oxygen Content, $3 + \delta$), Synthesis Conditions (Q: Sample Quenched from the Given Conditions—All Other Samples Slowly Cooled), Valency of Manganese (v(Mn), Calculated According to $v(\mathrm{Mn}) = 3 + 2\delta + 3t$), Unit Cell Dimensions (PXD at 298 K, Last Digit Uncertain) for $La_{1-t}MnO_{3+\delta}$, Structure Type at 298 K, Type of Magnetic Order at 9 K (F Ferro-, AF Antiferromagnetic with Small Ferromagnetic Component), and Magnetic Ordering Temperature (from PND, ±5–10 K)

$1 - t$	$3 + \delta$	Atm.	T(K)	v(Mn)	a(pm)	b(pm)	c(pm)	α(°)	Type	Magn.	$T_{N,C}$(K)
1.00	3.00	CO_2/H_2	1270	3.00	573.4	770.3	554.0		ORT1	AF	140
	3.08	air, Q	1273	3.16	549.7	779.4	553.2		ORT2	F	125
	3.15	air	1023	3.30	546.7			60.726	RH[a]	(F)	[b]
0.96	2.94	CO_2/H_2	1270	3.00	573.2	769.0	553.7		ORT1	AF	[c]
	3.05	O_2	1023	3.22	547.4			60.640	RH	F	213
0.92	2.88	CO_2/H_2	1270	3.00	573.0	769.5	553.4		ORT1	AF	143
0.88	2.82	CO_2/H_2	1270	3.00	572.5	769.8	553.7		ORT1	AF	143
	2.92	O_2	1023	3.20	547.6			60.540	RH	F	248

[a] ORT2-type at 9 K.
[b] No transition, see text.
[c] Not measured.

in air from high temperatures (say 1300 K). Both the ORT1- and ORT2-type samples crystallize in space group *Pnma.* The ORT2-type has almost equal a and c axes, whereas for the ORT1-type these axes differ by some 3% ($a > c$; cf. Table 1). The orthorhombic splittings in PXD/PND patterns for the ORT2-type samples are small, and the patterns may easily be erroneously indexed on a rhombohedral cell with α around 60.15°.

The magnetic susceptibility for $La_{0.96}MnO_{3.05}$ shown in Fig. 1 is representative for RH-type samples. Samples of this type are ferromagnetic and for $La_{0.96}MnO_{3.05}$, T_C = 165 ± 3 K (Fig. 1, inflection point).

The magnetic susceptibility for $LaMnO_{3.00}$ (Fig. 2) is typical for ORT1-type samples under FC conditions. For ZFC samples *different* behaviors are found as further discussed in (23). In several cases typical antiferromagnetic (AF) behaviour with a cusp in the susceptibility around 135 K is observed (Fig. 2). The difference in behavior between ZFC and FC samples indicates that a small ferromagnetic component is induced on field cooling. Hence, these are all ferrimagnetic. The ferromagnetic component saturates in weak magnetic fields, but no overall saturation is obtained for $H \leq 50$ kOe; see inset to Fig. 2. The spontaneous magnetic moment vanishes on heating in zero field at the AF ordering temperature. The ferromagnetic components at 5 K for ORT1-type samples are less than 0.4 μ_B. This agrees with the findings by Elemans *et al.* (8), where magnetization data give a moment of 0.1 μ_B and PND data are consistent with a moment $\mu_F = 0.0 \pm 0.2$ μ_B (refinements gave $\mu_F = 0.5 \pm 0.2$ μ_B).

The magnetic susceptibility data for $LaMnO_{3.08}$ in Fig. 3 are typical for ORT2-type samples and indicate ferromagnetic order below the Curie temperature, $T_C = 110 \pm 5$ K (inflection point). The $1/H$ extrapolated saturation magnetization at 5 K is 79 e.m.u./g (3.35 μ_B), see inset to Fig. 3.

Magnetic phase diagram and susceptibility data for the entire nonstoichiometric range for $La_{1-t}MnO_{3+\delta}$, including samples (subgroup of ORT1-type samples) giving apparent negative magnetizations, will be presented separately (23).

(*ii*) *Crystal structure at 9 K; temperature induced struc-*

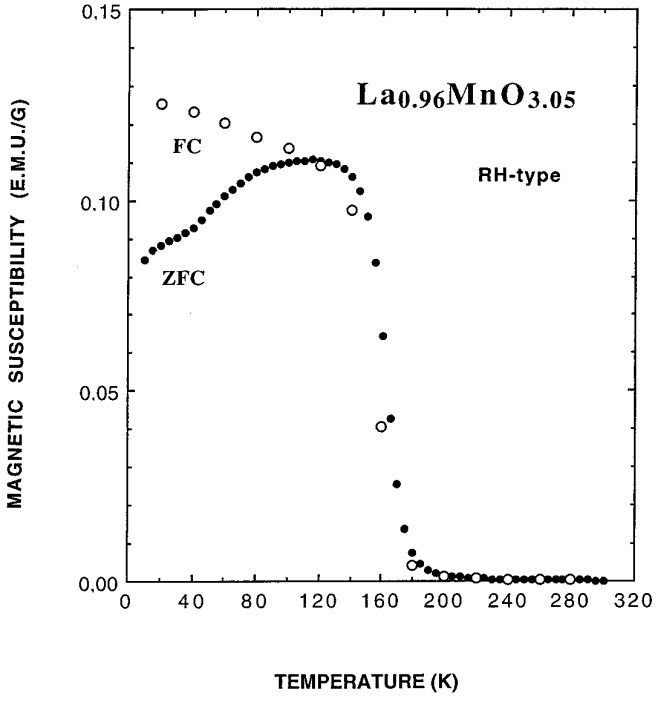

FIG. 1. Magnetic susceptibility versus temperature for $La_{0.96}MnO_{3.05}$ (RH-type).

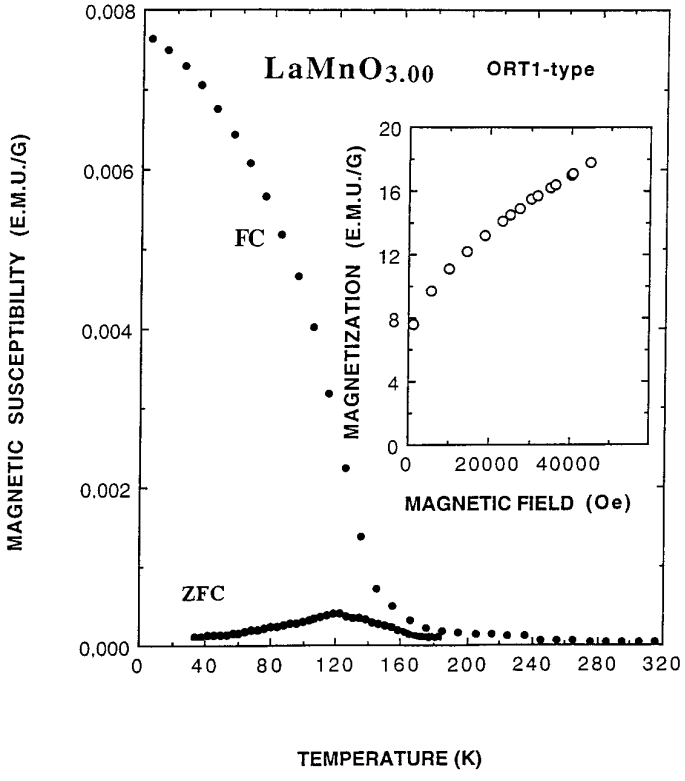

FIG. 2. Magnetic susceptibility (ZFC and FC) versus temperature for $LaMnO_{3.00}$ (ORT1-type). Inset shows magnetization for fields $H \leq 50$ kOe.

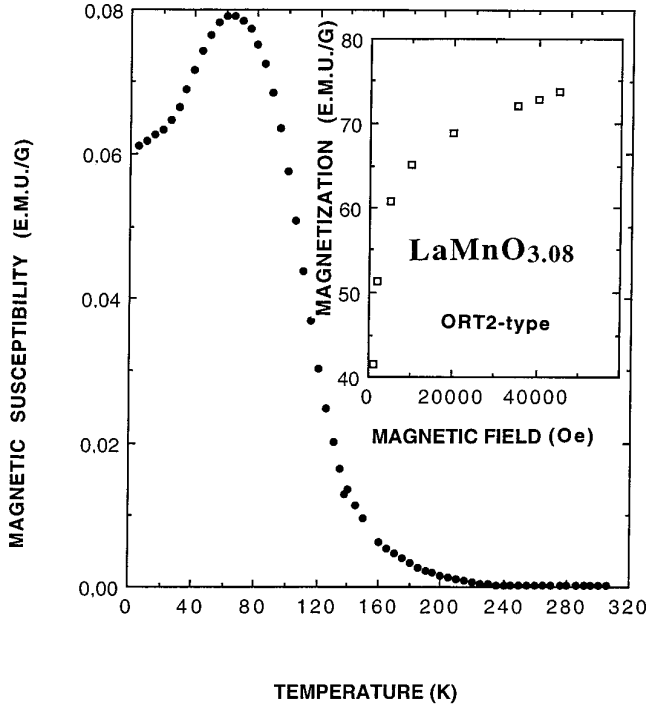

FIG. 3. Magnetic susceptibility versus temperature for $LaMnO_{3.08}$ (ORT2-type). Inset shows magnetization for fields $H \leq 50$ kOe.

TABLE 2

Atomic Coordinates, Occupation Numbers and Magnetic Moments for the Rhombohedral Variant (RH) of $La_{1-t}MnO_{3+\delta}$ at $T = 9$ K as Derived from Rietveld Refinements of Powder Neutron Diffraction Data Collected at the JEEP II Reactor, Kjeller

	$La_{0.96}MnO_{3.05}$	$La_{0.88}MnO_{2.92}$[a]
a (pm)	546.11(8)	545.69(7)
α (°)	60.636(4)	60.604(4)
x_O	0.8005(6)	0.7988(6)
$\mu_\parallel$ (μ_B)	1.43(25)	2.39(12)
$\mu_\perp$ (μ_B)	3.03(14)	2.49(11)
μ_F (μ_B)	3.93(10)	4.22(6)
R_n	6.14	5.27
R_m	7.26	3.98
R_p	12.69	9.86

Note. Magnetic components parallel and perpendicular to unique rhombohedral axis ([111]) are given. Calculated standard deviations in parentheses. Nuclear, magnetic, and profile R-factors are given. Space group $R\bar{3}c$, La in 2(a) [¼, ¼, ¼], Mn in 2(b) [0, 0, 0], and O in 6(e) [x, $-x + ½$, ¼].

[a] Slight impurities of Mn_3O_4 detected by PXD, hardly observable by PND.

tural phase transitions. Positional parameters, displacement factors, occupation numbers and magnetic moments were derived from Rietveld-type refinements. Owing to strong correlations and a limited $\sin\Theta/\lambda$ range, several parameters were fixed or constrained during stages of the refinements. The obtained results are listed in Tables 2–4.

According to earlier studies (15, 16), no interstitial atoms are directly involved in the defect structure for lanthanum manganite. Hence, the occupancies for La, Mn, and O could be constrained to fit the nominal composition during the refinements. For $t = 0.12$, slight impurities of Mn_3O_4 were present. In that case, the occupancy for La was refined, whereas those for oxygen were constrained via the La occupancy.

As can be read from Tables 1 and 3, the structural state for $LaMnO_{3.15}$ changes from RH-type at 298 to ORT2-type at 9 K. At first sight, $LaMnO_{3.15}$ appeared at 9 K still to have the RH-type structure, and refinements could be carried out fairly well in space group $R\bar{3}c$ with α around 60.15°. However, the weak additional peaks present at, e.g., $2\Theta = 52.0$, 57.8, and 64.9° in the PND diagram at 9 K (marked by arrows in Fig. 4) prove that the correct space group is *Pnma* and that the structure is of ORT2-type.

The temperature for the ORT2- to RH-type phase transition, $T_d = 200 \pm 20$ K, was determined from the temperature dependence of selected reflections. The (122)/(211) reflections at $2\Theta = 52.0°$ served as trademark for the ORT2-type (cf. Fig. 4), whereas broadening/splitting of the strong reflection around $2\Theta = 48°$ (cf. Fig. 4) served to identify the RH-type modification. The first order struc-

TABLE 3

Atomic Coordinates, Occupation Numbers, and Magnetic Moments for the Orthorhombic ORT2 Variant of $La_{1-t}MnO_{3+\delta}$ at $T = 9$ K as Derived from Rietveld Refinements of Powder Neutron Diffraction Data Collected at the JEEP II Reactor, Kjeller

	$La_{1.00}MnO_{3.15}$	$La_{1.00}MnO_{3.08}$
a (pm)	547.24(6)	550.22(11)
b (pm)	775.43(16)	777.44(16)
c (pm)	551.30(9)	552.10(18)
x_{La}	0.0209(9)	0.0275(8)
z_{La}	0.9943(9)	0.9879(13)
x_{O1}	0.4937(14)	0.4941(14)
z_{O1}	0.0538(16)	0.0617(17)
x_{O2}	0.2315(12)	0.2288(19)
y_{O2}	0.5357(7)	0.5355(8)
z_{O2}	0.2284(11)	0.2227(15)
μ_{Fy} (μ_B)	0.80(7)	2.46(4)
R_n	4.31	6.78
R_m	11.80	4.47
R_p	9.25	8.71

Note. Calculated standard deviations in parentheses. Nuclear, magnetic, and profile R-factors are given. Space group *Pnma*; La and O(1) in 4(c) [x, $\frac{1}{4}$, z], Mn in 4(a) [0, 0, $\frac{1}{2}$], and O(2) in 8(d) [x, y, z].

tural transition does not coincide with onset of magnetic order. The diffraction peaks are broadened in an interval around T_d, possibly indicating coexistence of the two phases or inhomogeneity with respect to oxygen distribution. The transition in $LaMnO_{3.15}$ is similar to that for $LaCrO_3$ where the ORT2- to RH-type transition occurs at 550 K, whereas AF order (G_x type) first occurs below 290 K (30). The findings for $LaMnO_{3.15}$ fit further the early report by Wold and Arnott (31) on composition-dependent structural phase transitions for lanthanum manganite. Mahesh *et al.* (12) recently reported that rhombohedral $LaMnO_{3+\delta}$ undergoes a metal–insulator transition (referring solely to the temperature dependence of the resistivity) just below the Curie temperature. The same was reported for cubic $LaMnO_{3+\delta}$ obtained via a different precursor-based synthesis (32). In view of the present data, the ''metal–insulator'' transition appears to be connected with the first order structural transition.

The refined positional parameters for the ORT1- and ORT2-type samples in Tables 3 and 4 differ significantly. As a consequence, the distortions of the MnO_6 octahedra are quite different for the two types. Interatomic distances are listed in Table 5. The MnO_6 octahedra are fairly symmetrical for the RH- and ORT2-types, whereas they are heavily distorted into a (2 + 2) + 2 situation for the ORT1-type.

(*iii*) *Magnetic structure at 9 K and order–disorder transitions.* Additional magnetic scattering is present at low temperatures for all PND samples, with some exception for $LaMnO_{3.15}$. The ordering temperatures were determined from the temperature dependence of the integrated intensity of selected reflections, see Fig. 5 and Table 1. Parameters describing the magnetic structures were derived from Rietveld-type analyses of the PND data, see Tables 2–4. The ordering temperatures were determined from linear extrapolation of $I_{mag}(T)$ to background level, and devia-

TABLE 4

Atomic Coordinates, Occupation Numbers, and Magnetic Moments for the Orthorhombic ORT1 Variant of $La_{1-t}MnO_{3+\delta}$ at $T = 9$ K as Derived from Rietveld Refinements of Powder Neutron Diffraction Data Collected at the JEEP II Reactor, Kjeller

	$La_{1.00}MnO_{3.00}$	$La_{0.96}MnO_{2.94}$	$La_{0.92}MnO_{2.88}$	$La_{0.88}MnO_{2.82}$
a (pm)	572.98(6)	572.37(11)	571.87(9)	572.16(10)
b (pm)	767.22(10)	765.95(18)	766.95(14)	767.58(17)
c (pm)	553.63(6)	552.57(11)	552.84(8)	553.09(10)
x_{La}	0.0497(11)	0.0521(17)	0.0475(12)	0.0452(13)
z_{La}	0.9949(11)	0.9939(15)	0.9939(12)	0.9939(15)
x_{O1}	0.4880(13)	0.4829(18)	0.4848(15)	0.4829(18)
z_{O1}	0.0732(13)	0.0736(19)	0.0719(14)	0.0689(16)
x_{O2}	0.1942(8)	0.1906(10)	0.1930(8)	0.1906(9)
y_{O2}	0.5418(7)	0.5413(10)	0.5401(8)	0.5413(9)
z_{O2}	0.2266(12)	0.2228(16)	0.2265(13)	0.2253(14)
μ_{Ax} (μ_B)	3.42(3)	3.41(4)	3.38(3)	3.24(3)
R_n	6.06	5.75	5.75	7.63
R_m	8.50	9.67	6.98	10.27
R_p	15.80	20.43	17.02	20.05

Note. Calculated standard deviations in parentheses. Nuclear, magnetic, and profile R-factors are given. Space group *Pnma*; La and O(1) in 4(c) [x, $\frac{1}{4}$, z], Mn in 4(a) [0, 0, $\frac{1}{2}$], and O(2) in 8(d) [x, y, z].

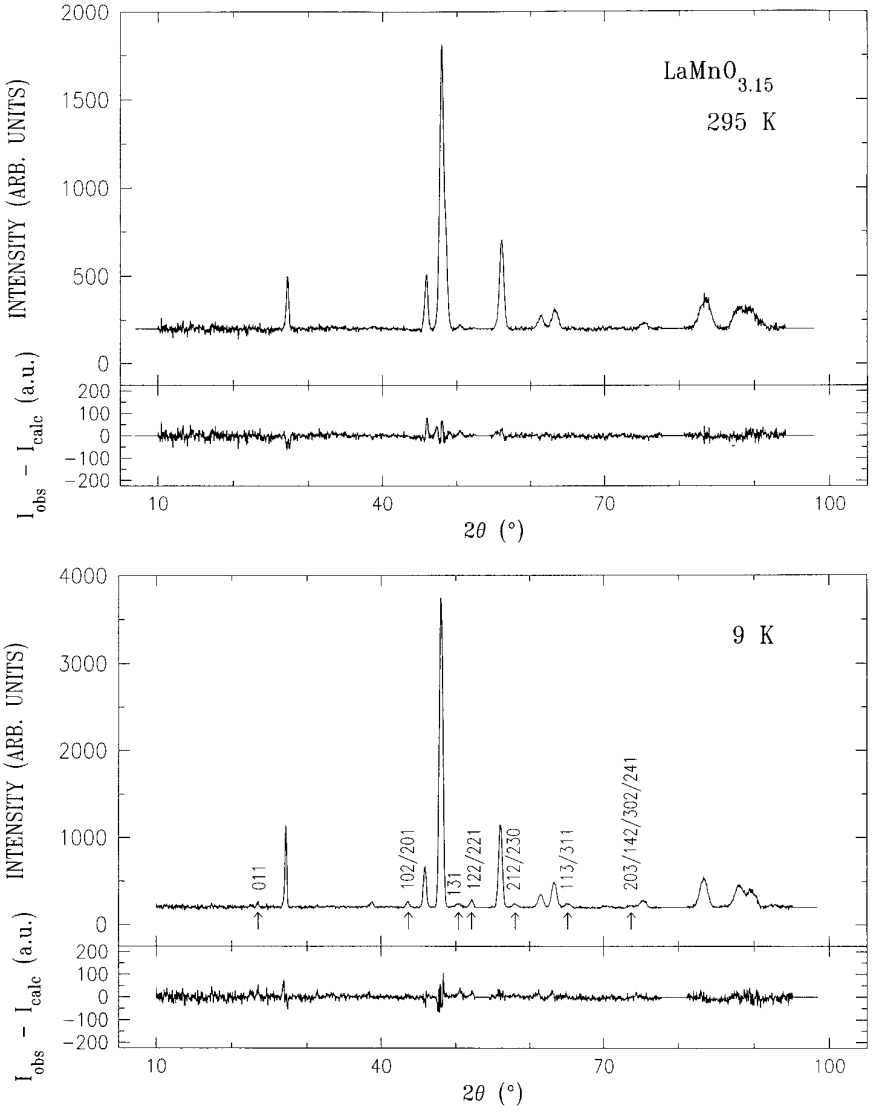

FIG. 4. Observed and difference powder neutron diffraction pattern for $LaMnO_{3.15}$ at 298 K (RH-type) and at 9 K (ORT2-type), $\lambda = 182.5$ pm. Additional reflections occurring for the ORT2-type at 9 K are marked by arrows and Miller indices are given.

tions between susceptibility and PND results are simply consequences of the way chosen to define transition temperatures.

At 9 K all the RH-type samples are purely ferromagnetic. The magnetic moments are inclinded to the unique axis, [111], for $La_{0.96}MnO_{3.05}$ and $La_{0.88}MnO_{2.92}$ (Table 2). Observed intensities and difference between observed and calculated PND intensities are shown for $La_{0.96}MnO_{3.05}$ in Fig. 6.

The ORT2-type samples are also ferromagnetically ordered, Table 3. The magnetic moments are parallel to [010]. The magnetic structure belongs to an F_y mode. Observed intensities and difference between observed and calculated PND intensities are shown for $LaMnO_{3.15}$ in Fig. 4.

For the ORT1-type samples, additional magnetic scattering is observed for reflections with $h + l = 2n$ and $k = 2n + 1$. The antiferromagnetic component is of A_x-type (Table 4), meaning that four neighboring Mn are ferromagnetically and two are antiferromagnetically coupled. The weak ferromagnetic components of the ferrimagnetic structures for the ORT1-type samples (see above) were too small to be detected by PND. Hence, the direction of the ferromagnetic moments could not be determined. It is possible that the ferromagnetism is of F_y-type, corresponding to that found for the more oxidized, but not Jahn–Teller distorted, samples. (The A_x and F_y modes transform according to the same irreducible representation; magnetic space group $Pn'm\,a'$ (4)). Observed and difference PND intensities are shown for $LaMnO_{3.00}$ in Fig. 7.

The oxidation state of manganese in the ORT1-type

TABLE 5

Calculated Distances (in pm) for Selected Samples of $La_{1-t}MnO_{3+\delta}$ Based on Unit Cell Dimensions and Atomic Coordinates Determined from PND Data at 9 K

	$LaMnO_{3.15}$ (ORT2)	$La_{0.96}MnO_{3.05}$ (RH)	$LaMnO_{3.00}$ (ORT1)
La–O2 (2×)	248.5	247.8	243.3
–O1 (1×)	249.6	247.8	242.2
–O2 (2×)	259.7	274.5	264.0
–O1 (1×)	260.8	274.5	250.5
–O2 (2×)	281.1	274.5	268.4
–O1 (1×)	290.4	274.5	316.1
–O1 (1×)	302.5	303.5	328.8
–O2 (2×)	312.3	303.5	342.2
Mn–O2 (2×)	195.5	196.0	190.7
–O1 (2×)	196.1	196.0	196.0
–O2 (2×)	198.1	196.0	218.0

Note. O1 and O2 equivalent for the RH-type. Typical calculated standard deviations in La–O distances 1.0 pm, in Mn–O distances 0.2 pm.

samples is +3. Under this valency constraint, the ordering temperature and the magnetic moment appear to be independent of the chemical composition. The structural changes for $La_{1-t}MnO_{3+\delta}$ involve lanthanum and oxygen vacancies. As long as the introduced lack of positive and negative charge balances, the magnetic properties are unaffected. This is analogous to what found for reduced $La_{1-t}Ca_tCrO_{3-t/2}$ (30), for which the magnetic moment and Néel temperature remain unaltered at modest substitution levels.

The A_x order in Jahn–Teller distorted $REMnO_{3+\delta}$ (RE = La, Pr, Nd, Sm, Eu, Gd, Tb, Dy, and Ho (5)) is explained by AF superexchange interactions along [010] and ferromagnetic exchange between empty and filled e_g orbitals within the *ac*-plane (33–35). Introduction of Mn^{IV} via oxidation or aliovalent substitution favours double exchange and ferromagnetic couplings (11). At the same time, the Jahn–Teller distortion is weakened; cf. $Pr_{1-t}Ba_tMnO_3$ and $La_{1-t}Ca_tMnO_3$ (1, 36), where the relative amounts of Mn^{III} and Mn^{IV} species are controlled by substitution and atmosphere during synthesis. For $La_{1-t}Ca_tMnO_3$, Wollan and Koehler (1) observed the breakdown of the cooperative Jahn–Teller distortion for 15–20% Mn^{IV}. The same situation is described here for $La_{1-t}MnO_{3+\delta}$ itself.

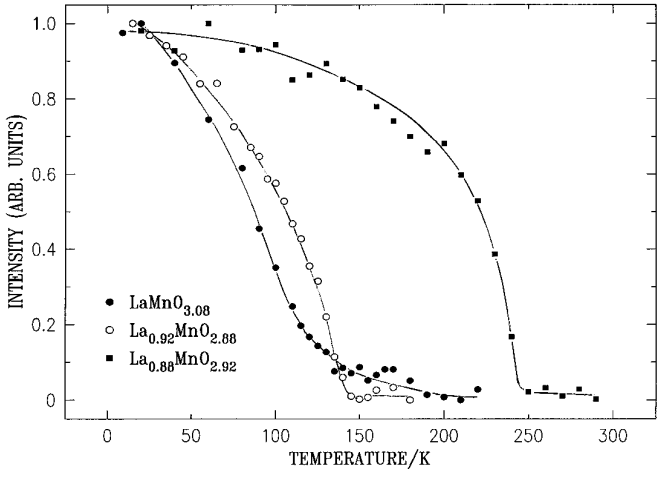

FIG. 5. Temperature dependence of the integrated intensity for the 101 reflection for $LaMnO_{3.08}$ (ORT2-type), the 010 reflection for $LaMnO_{3.00}$ (ORT1-type), and the 101 reflection for $La_{0.88}MnO_{2.92}$ (RH-type; nominal composition).

The ordered magnetic moment for Mn differs substantially among the different PND samples. The same form factor (Mn^{3+}) was selected for all refinements in order to facilitate comparison. For the RH-type samples, $\mu_F \approx 4\ \mu_B$ (Table 2), which is higher than expected for 20% Mn^{IV} and $L = 0$ (spin only). For the ORT1-type samples with solely Mn^{III}, the antiferromagnetically ordered moment is around 3.4 μ_B. In addition, magnetization data show a ferromagnetic component of ~0.4 μ_B. The latter feature has been considered as intrinsic to stoichiometric $LaMnO_3$ (3, 7–11). It is reasonable to believe that defects (La vacancies, Mn^{IV} species) giving rise to local spin distortions are the origin for the *F*-component (11). Parasitic ferromagnetism is also reported for solid solution phases such as $La_{0.875}Ba_{0.125}Mn_{0.875}Ti_{0.125}O_3$ with a claimed average Mn oxidiation state of +3 (8). However, the very controlling of the nonstoichiometry during synthesis, together with a small, yet existing, tendency toward reoxidation in air, makes it very difficult from a synthetic and handling point of view to produce large-scale 100% stoichiometric samples. Even slight amounts of the divalent impurities inevitably introduced from the reagents will cause formation of Mn^{IV}. This implies that double exchange will be operative locally. It should be added that recent defect models point at another possible source for different oxidation states, namely charge disproportionation of Mn^{III} into Mn^{II} and Mn^{IV} (17), at least at elevated temperatures.

The results for the ORT2-type samples are quite surprising. For $LaMnO_{3.08}$, the ferromagnetic moment is rather small, $\mu_F = 2.5\ \mu_B$; however, for $LaMnO_{3.15}$, the ordered moment appears almost to vanish, $\mu_F = 0.8\ \mu_B$ (Table 3), i.e., far less than expected for any Mn^{III}/Mn^{IV} mixture. In order to be confident of the sample quality and the result, the PND experiment for $LaMnO_{3.15}$ was repeated after 6 months; however, this confirmed the situation. There is no indication of second phases, additional peaks owing to AF order, or low-angle satellite reflections. The 101 reflection appears from refinements (F_y mode) and temperature variation to have the largest magnetic intensity contribution. The integrated intensity for this reflection shows only a smooth decrease with

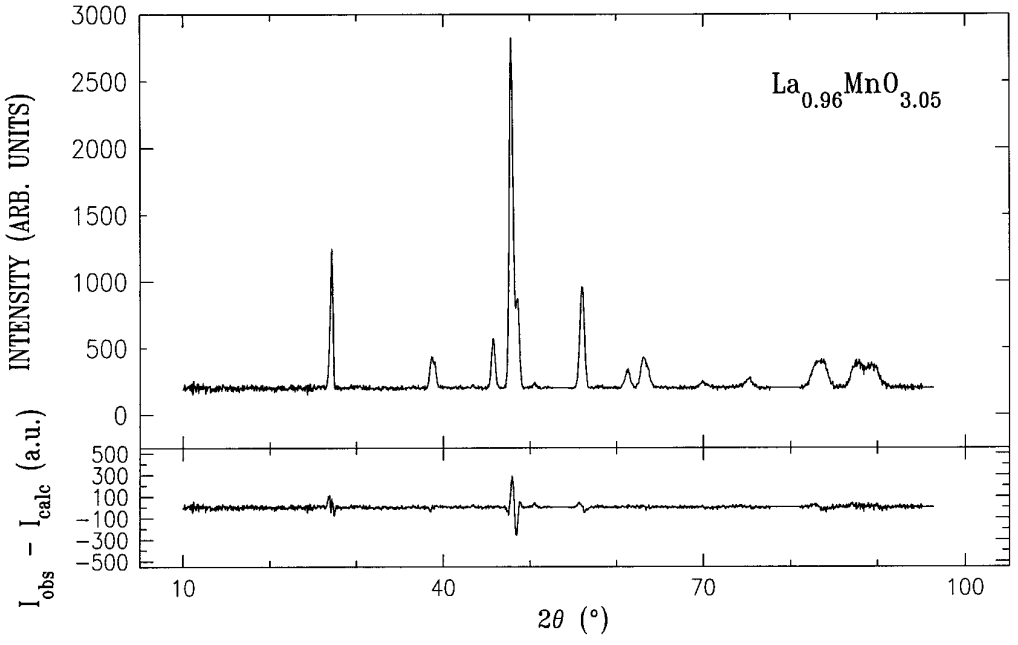

FIG. 6. Observed and difference powder neutron diffraction pattern for $La_{0.96}MnO_{3.05}$ (RH-type) at 9 K, $\lambda = 182.5$ pm.

increasing temperature. This indicates that the ordered moment at 9 K in reality is much less, if present at all, than 0.8 μ_B (Table 3) which is a result of counting statistics and introduction of additional variables in the least-squares refinements. Magnetic susceptibility data for $LaMnO_{3.15}$ are given in Fig. 8. We believe that the cusp in the curve for ZFC samples is connected with frozen spins rather than long range order. For $LaMnO_{3.15}$, 30% of the manganese atoms are tetravalent, the rest being trivalent. It is currently believed that the lattice symmetry and the number of *AF* and *F* couplings cause a frustrated system exhibiting spin-glass features.

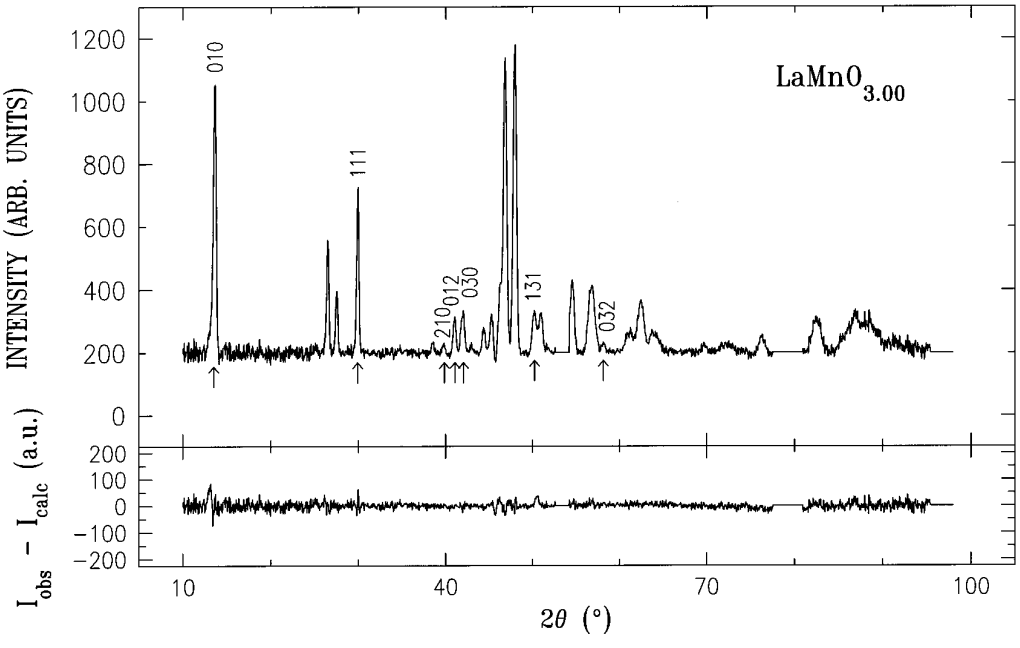

FIG. 7. Observed and difference powder neutron diffraction pattern for $LaMnO_{3.00}$ (ORT1-type) at 9 K, $\lambda = 182.5$ pm. Miller indices for magnetic reflections marked by arrows are given.

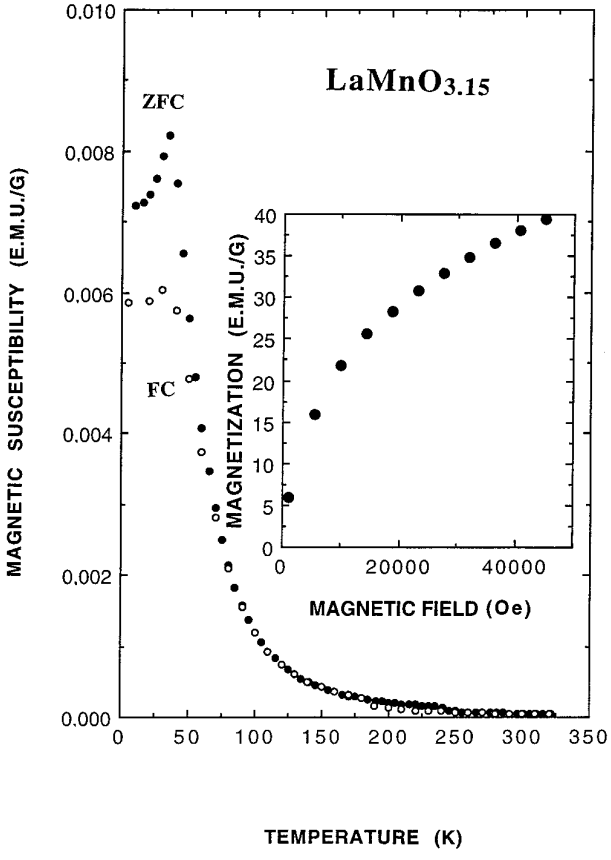

FIG. 8. Magnetic susceptibility for zero field cooled (ZFC, filled symbols) and field cooled (FC, open symbols) $LaMnO_{3.15}$. Insert shows magnetization for $H \leq 50$ kOe.

CONCLUSION

1. ORT1-type samples with large amounts of Mn^{III} are Jahn–Teller distorted. The magnetic order is of A_x-type with small additional parasitic ferromagnetism. The Néel temperature (135 K) and magnetic moments (3.4 μ_B) are not affected by La deficiency as long as the Mn valency is constant.

2. ORT2-type samples with some 15% Mn^{IV} are ferromagnetically ordered (F_y-mode). Their moments ($<2.5\ \mu_B$) are lower than for the ORT1-type samples.

3. RH-type samples order ferromagnetically with a large moment (3.9 μ_B) and have the highest Curie temperatures among the modifications. They show large variation in ordering temperature with nonstoichiometry.

4. For $LaMnO_{3.15}$ no, or very slight, cooperative magnetic order is present at 10 K, indicating a spin-glass situation.

5. For $LaMnO_{3.15}$ a temperature-induced $RH\text{-} \rightarrow O'RT2$-type transition occurs on cooling to around 200 K.

ACKNOWLEDGMENT

This work has received financial support from the Research Council of Norway.

REFERENCES

1. E. O. Wollan and W. C. Koehler, *Phys. Rev.* **100,** 545 (1955).
2. W. C. Koehler and E. O. Wollan, *J. Phys. Chem. Solids* **2,** 100 (1957).
3. G. Matsumoto, *J. Phys. Soc. Jpn.* **29,** 606 (1970).
4. E. F. Bertaut, *Acta Crystallogr. Sect. A* **24,** 217 (1968).
5. A. Olés, A., F. Kajzar, M. Kucab, and W. Sikora, "Magnetic Structures Determined by Neutron Diffraction." Polska Akademia Nauk, Warsaw, Krakow, 1976.
6. R. Pauthenet and C. Veyret, *J. Phys.* (*Paris*) **31,** 65 (1970).
7. F. K. Lotgering, *Philips Res. Rep.* **25,** 8 (1970).
8. J. B. A. A. Elemans, B. van Laar, K. R. van der Veen, and B. O. Loopstra, *J. Solid State Chem.* **3,** 238 (1971).
9. G. Matsumoto, *J. Phys. Soc. Jpn.* **29,** 615 (1970).
10. C. Zener, *Phys. Rev.* **82,** 403 (1951).
11. P. G. de Gennes, *Phys. Rev.* **118,** 141 (1960).
12. R. Mahesh, K. R. Kannan, and C. N. R. Rao, *J. Sol. State Chem.* **114,** 294 (1995).
13. T. Sasaki, Y. Matsumoto, J. Hombo, and Y. Ogawa, *J. Solid State Chem.* **91,** 61 (1991).
14. H. Fjellvåg, O. H. Hansteen, B. Gilbu, A. Olafsen, N. Sakai, and H. Seim, *Thermochim. Acta* **256,** 75 (1995).
15. J. A. M. van Roosmalen, E. H. P. Cordfunke, R. B. Helmholdt, and H. W. Zandbergen, *J. Solid State Chem.* **110,** 100 (1994).
16. B. C. Tofield and W. R. Scott, *J. Solid State Chem.* **10,** 183 (1974).
17. J. A. M. van Roosmalen and E. H. P. Cordfunke, *J. Sol. State Chem.* **110,** 109 (1994).
18. K. Kamata, T. Nakajima, T. Hayashi, and T. Nakamura, *Mater. Res. Bull.* **13,** 49 (1978).
19. J. H. Kuo, H. U. Anderson, and D. M. Spalin, *J. Solid State Chem.* **83,** 52 (1989).
20. J. Mizusaki, H. Tagawa, Y. Yonemura, H. Minamiue, and H. Nambu, *in* "Proceedings 2nd International Symposium on Ionic and Mixed Conducting Ceramics," (T. A. Ramaranayanan, W. L. Worrell, and H. L. Tuller, Eds.). *Electrochem. Soc. Proc.* **94-12,** 402 (1994).
21. N. Sakai and H. Fjellvåg, *Acta. Chem. Scand.,* in press.
22. N. Sakai, H. Fjellvåg, and B. Lebech, submitted for publication.
23. H. Fjellvåg and N. Sakai, to be published.
24. JCPDS, Powder Diffraction File No. 5-565.
25. N. O. Ersson, "Program CELLKANT." Department of Chemistry, University of Uppsala, Uppsala, 1981.
26. H. M. Rietveld, *J. Appl. Crystallogr.* **2,** 65 (1969).
27. A. W. Hewat, "The Rietveld Computer Program for the Profile Refinement of Neutron Diffraction Powder Patterns Modified for Anisotropic Thermal Vibrations." UKAERE Harwell Report RRL 73/897, 1973.
28. L. Koester and H. Rauch. IAEA Contract 2517/RB, IAEA, Vienna, 1981.
29. R. E. Watson and A. J. Freeman, *Acta Crystallogr.* **14,** 27 (1961).
30. N. Sakai, H. Fjellvåg, and B. C. Hauback, *J. Solid State Chem.* **121,** 200 (1996).
31. A. Wold and R. J. Arnott, *J. Phys. Chem. Solids* **9,** 176 (1959).
32. M. Verelst, N. Rangavittal, C. N. R. Rao, and A. Rousset, *J. Solid State Chem.* **104,** 74 (1993).
33. J. Kanamori, *J. Phys. Chem. Solids* **10,** 87 (1959).
34. J. B. Goodenough, A. Wold, R. J. Arnott, and N. Menyuk, *Phys. Rev.* **124,** 573 (1961).
35. P. W. Anderson, *Phys. Rev.* **115,** 2 (1959).
36. E. Pollert and Z. Jirak, *J. Solid. State Chem.* **35,** 262 (1980).